Impact of topography, climate and moisture sources on isotopic composition (δ 18 O & δ D) of rivers in the Pyrenees: Implications for topographic reconstructions in small orogens

Damien Huyghe, Frédéric Mouthereau, Mathieu Sebilo, Arnaud Vacherat, Loïc Ségalen, Patricia Richard, Philippe Biron, Thierry Bariac

Impact of topography, climate and moisture sources on isotopic composition ($\delta^{18}O$ & δD) of rivers in the Pyrenees: implications for topographic reconstructions in small orogens

Damien Huyghe[1,2], Frédéric Mouthereau[1], Mathieu Sébilo[3], Arnaud Vacherat[1], Loïc Ségalen[4], Patricia Richard[3], Philippe Biron[3], Thierry Bariac[3]

[1] Géosciences Environnement Toulouse (GET), Université Paul Sabatier Toulouse 3, 14 Avenue Edouard Belin, 31400 Toulouse, France

[2] Now at Sorbonne Universités, UPMC-Paris 06, UMR 8222, Lab. Ecogéochimie des environnements benthiques (LECOB), Observatoire Océanologique, F-66650, Banyuls-sur-mer, France

[3] Sorbonne Université UPMC Université Paris 06, Institut d'Ecologie et des Sciences de l'Environnement de Paris (IEES Paris), CNRS, Campus INRA, AgroParisTech, Bâtiment EGER, 78550 Thiverval-Grignon, France

[4] Sorbonne Universités, UPMC-Paris 06, UMR CNRS 7193, ISTeP, F-75005, Paris, France

Abstract

Understanding how orogenic topography controls the spatial distribution and isotopic composition of precipitation is critical for paleoaltitudinal reconstructions. Here, we determine the isotopic composition ($\delta^{18}O$ and δD) of 82 small rivers and springs from small catchments in the Pyrenees. Calculation of the deuterium excess (d-excess) parameter allows the distinction of four distinct isotopic provinces with d-excess values of between 15 and 22 ‰ in the northwest, between 7 and 14 ‰ in the central northern Pyrenees and between 3 and 11 ‰ in the northeast. The southern Pyrenees have a homogenous d-excess signature ranging from 7 to 14 ‰. Our results show significant local moisture recycling and/or rain amount effect in the northwestern Pyrenees, and control by evaporation processes during rainfall events in the southern Pyrenees and for low elevated samples of the northeast of the range. Based on the distribution of d-excess values, we estimate contrasting isotope lapse rates of -2.9/-21.4 ‰/km ($\delta^{18}O/\delta D$) in the northwest, -2.7/-21.4 ‰/km ($\delta^{18}O/\delta D$) in the north central and -3.7/-31.7 ‰/km ($\delta^{18}O/\delta D$) in the northeastern Pyrenees. The southern Pyrenees show distinctly higher lapse rates of -9.5/-77.5 ‰/km ($\delta^{18}O/\delta D$), indicating that in this area the altitudinal effect in not the only parameter driving isotopic composition of rivers. Despite their relatively low topographic gradient, the Pyrenees exert a direct control on the isotopic composition of river waters, especially on their northern side. The variations in isotopic composition-elevation relationships documented along the strike of the range are interpreted to reflect an increasing continentality effect driven by wind trajectories parallel to the range, and mixing with Mediterranean air masses. Despite these effects, the measurable orographic effect on precipitation in the Pyrenees proves that the isotopic composition approach for reconstructing past topography is applicable to low-elevation orogens.

Keywords: stable isotopes; orographic effect; paleoaltimetry; meteoric water; western Europe; climate

1. Introduction

Topography of continents is the expression of the coupling processes between geodynamics that govern exhumation, loading and unloading of the continental crust and earth surface processes (Mulch et al., 2016). These processes control ways in which sediments are stored and transported from mountainous areas to sink domains (e.g. Allen, 2008). The elevation of mountain ranges exerts a direct control on atmospheric circulation and thus on precipitation and climate, and has strong implications on topics as broad as geodynamics, tectonics, sedimentology, paleoclimatology or paleontology (Mulch, 2016). Documenting the evolution of Earth's surface elevation is a critical question for understanding the tectonic evolution of collisional domains, and to investigate tectonics vs climate interactions and their relative influence on erosion and sedimentation (Rowley and Garzione, 2007).

Paleoaltitudes have successfully been reconstructed for highly elevated domains like the Andean Plateau (e.g. Garzione et al., 2014) or the Himalaya and Tibetan Plateau (Caves et al., 2015; Gébelin et al., 2013) and less elevated mountains ranges like the Sierra Nevada (Mulch et al, 2016), the Alps (Campani et al., 2012) and the Pyrenees (Huyghe et al., 2012a). The fundamental principle lies in the fact that both the isotopic composition in oxygen ($\delta^{18}O$) and hydrogen (δD) in rain decreases with elevation. This first-order relationship reflects a simple Rayleigh distillation behaviour in which rainfall is increasingly depleted in the heavy isotopes (^{18}O and D) with elevation (Dansgaard, 1964; Gonfiantini et al., 2001; Rowley, 2007). The rate at which this decrease occurs is measured on modern water (i.e., the isotopic

73 lapse rate) and can then be converted to paleoelevation fluctuations as variations of the
74 isotopic signature of minerals formed from meteoric water can be related, in principle, to a
75 combination of climatic and elevation changes. (e.g., Rowley et al., 2001).

76 However, limitations have to be considered when interpreting the isotopic composition
77 of minerals as a measure of paleoaltimetry. In particular, topography may modify the pattern
78 of atmospheric circulation, leading to the isolation of two geographically distinct climatic
79 provinces characterized by specific isotopic fractionation that may cause changes in the $\delta^{18}O$
80 composition (Ehlers and Poulsen, 2009; Insel et al., 2012). In the case of a dominant
81 orographic effect, the windward side of the orogen experiences wet conditions, with the
82 precipitation of moist air masses that record a typical Rayleigh distillation behaviour. On the
83 contrary, the leeward side of the orogen is frequently characterized by the advance of dry air
84 resulting in a local rain shadow. Due to aridity, the surface moisture is recycled to the
85 atmosphere and suffers isotopic fractionation. Thus, precipitation related to this source of
86 moisture does not directly conform to Rayleigh distillation processes. Reliable
87 paleotopographic investigations are then only possible on the windward side of the range
88 (Schemmel et al., 2013; Bershaw et al., 2016).

89 Modern isotopic lapse rates have been well documented from rain or river waters
90 monitored for highly elevated mountain ranges like the Andes (Gonfiantini et al., 2001;
91 Bershaw et al., 2016), the Sierra Nevada (Ingraham and Taylor, 1991), the Tibetan Plateau
92 and Himalaya (Garzione et al., 2000; Chen et al., 2008; Caves et al., 2015), the Anatolian
93 Plateau (Schemmel et al., 2013) or the Alps (Longinelli and Selmo, 2003). These studies
94 yielded mean isotopic lapse rates of ~ -2.8 ‰/km and ~ -22 ‰/km for $\delta^{18}O$ and δD
95 respectively. Local deviations from these empirical relationships have been observed, and
96 interpreted to reflect continentality or latitudinal effects (Winnick et al., 2014; Caves et al.,
97 2015). Whether low-elevated orogens also produce measurable orographic effect on

precipitation or are high enough to cause the isolation of two distinct isotopic provinces is unclear. For example, in the case of the Alps, the isotopic lapse rate is ~ -2 ‰ / km for both the northern side in Switzerland and for the southern side in Italy (Longinelli and Selmo, 2003). This result is found independently of a shift of ~ 3‰ in $\delta^{18}O$ values observed between the two sides caused by the different moisture sources. Thus, even if the isotopic lapse rates are nearly the same on the windward side of most mountain ranges all around the world, the absolute isotopic values may vary for a given elevation. Moreover, tracking isotopes in precipitation via global circulation models suggests that temporal modifications in air mass composition due to climatic and topographic variations can modify the local isotopic lapse rate and the resulting isotope-in-precipitation patterns at high elevation (Ehlers and Poulsen, 2009). Due to these uncertainties it is first required to document the local modern isotopic lapse rate from which assumptions can be formulated regarding a possible orographic effect on precipitation.

Here we focus on the Pyrenees, a small collisional orogen. Its size is beneficial to isotopic studies as a reliable and geographically extensive sampling across the range can be performed. Past elevations changes in the Pyrenees have been investigated using isotopic measurements on Eocene marine molluscs (Huyghe et al., 2012a) and Neogene pollen floras (Suc and Fauquette, 2012), proving the great potential of these techniques for yielding paleoelevation reconstructions in the Pyrenees. However, none of these studies have focused on the modern isotope vs elevation relationships in this range, which is crucial to determine if low-elevated mountain ranges are capable of exerting a control on the isotopic composition of precipitation, as was argued by previous studies. Moreover, working on the Pyrenees introduces specific problematic aspects compared to many other mountain ranges like the Andes, the Himalaya or the Sierra Nevada, because the main source of moisture, which is located in the Atlantic Ocean, is only slightly oblique to the topography (Fig. 1A).

2. Geological setting

The Pyrenees are a doubly vergent collisional orogen resulting from collision between the Iberian and European plates from the Late Cretaceous to the Middle Miocene (Muñoz, 1992; Vergés et al., 2002). This range presents the advantage of having been well documented for several aspects, including tectonic (e.g. Muñoz, 1992; Vergés et al., 2002; Mouthereau et al., 2014), geomorphologic (Babault et al., 2005; Gunnell et al., 2008) or sedimentologic and exhumational (Christophoul et al., 2003; Huyghe et al., 2012b; Vacherat et al., 2017) evolution. These previous studies show that shortening and exhumation were fastest during the Eocene and Oligocene times (Sinclair et al., 2005). This led to an increase in both erosion rates in the growing mountain range and detrital sedimentation rates in the adjacent foreland basins (Huyghe et al., 2009, 2012b; Filleaudeau et al., 2012). The paleogeographic and sedimentologic histories of the two foreland basins are different during the collision (Vacherat et al., 2017). The northern Pyrenees has always remained connected to the Atlantic Ocean and to the Mediterranean Sea since the Oligocene. On the contrary, the South-Pyrenean foreland basin was open towards the Atlantic Ocean only up until the Late Eocene. The uplift of the Cantabrian mountain belt led to the closure of the basin connection with the Atlantic, which became internally-drained. In the Late Miocene, the basin reconnected to the Mediterranean Sea (Garcia-Castellanos et al., 2003; Vacherat et al., 2017). Due to the endorheic phase, the South-Pyrenean foreland accumulated sediments sourced from the growing topography, which ultimately led to a reduction of the slope of the rivers and their erosive effectiveness (Babault et al., 2005).

3. Modern topography and climate

The Pyrenean range is nearly 600 km long east-west and is maximum 150 km wide in a north-south direction, with a maximum elevation of 3404 m at the Pic d'Aneto (Fig. 1A). Smaller mountainous reliefs occur around the Pyrenean domain and also contribute to the regional pattern of atmospheric circulation and precipitation. In Spain, these are from west to east, the Cantabrian Range, which corresponds to the western prolongation of the Pyrenees on the northern coast of the Iberian Peninsula; the Iberian Range, corresponding to the southern border of the Ebro Basin, which was inverted between the Late Cretaceous and the Miocene; and the Catalan Coastal Range (Fig. 1A). In France, the Corbières and the Montagne Noire correspond to small massifs in the northeastern Pyrenees. The southern and the northern Pyrenean domains exhibit a contrasting topographic pattern in that the northern side exhibits a steeper mean slope with highly incised valleys, contrary to the southern flank that is wider with a more gentle mean slope. These differences mainly reflect the variable long-term response of river incision to base level changes. The northern Pyrenean rivers are connected to the Atlantic Ocean and the Mediterranean Sea, whereas the Ebro drainage system cuts across a former endorheic basin.

The precipitation pattern around the Pyrenees is primarily controlled by the distribution of the topography, with the highest mean annual precipitation (MAP) observed at the highest elevations (Fig. 2A). For the low elevation areas bordering the range, the highest MAP is observed along the Atlantic coast in the northwestern Pyrenees (1450 mm/yr in Biarritz) (Fig. 2C). Over the northern Pyrenean piedmont, precipitation strongly decreases eastwards until the Lannemezan Plateau (1047 mm/yr at Campistrous). Eastwards, in the northeastern Pyrenees, precipitation decreases and reaches 557 mm/yr along the Mediterranean coast, in the city of Perpignan. In the southern Pyrenees, MAP is maximum

along the Atlantic coast (1740 mm/yr in San Sebastian), then gradually decrease to the east (720 mm/yr in Pamplona and 370 mm/yr in Huesca). MAP increases slightly in the southeastern Pyrenees, with 685 mm/yr in Girona along the Mediterranean coast. MAP is thus lower in the southern Pyrenean piedmont than in the northern one.

The main source of moisture over the Pyrenees is the northern Atlantic and related to the North Atlantic Oscillations (Fons, 1979; Lambs et al., 2003; Araguas-Araguas and Diaz Teijeiro, 2005). However, moisture can also be sourced from the western Mediterranean Sea and northern Europe (Lambs et al., 2003; Araguas-Araguas and Diaz Teijeiro, 2005). To accurately determine the origin of the moisture over the Pyrenees, we used the HYbrid Single-Particle Lagrangian Integrated Trajectory Model (HYSPLIT) (Stein et al., 2015) to track air parcel trajectories around the main topography (Fig. 1B to 1F). We selected five locations, three on the northern side of the range and two in the southern side, so as to cover the entire analysed domain for isotopic composition. We computed 72h back trajectories every 12h for each location, for the months of April and May 2013. These are the rainiest of the year, before the dry season, during which we sampled river waters. In this analysis, we only report trajectories that provided precipitation over the Pyrenees, representing a maximum of 471 trajectories in the northwest to a minimum of 156 to the southeast of the range. These data clearly indicate that the Atlantic Ocean is the main source of moisture for the rain sourcing the Pyrenean rivers, and that Mediterranean and northern European sources are limited in comparison.

Mean annual temperatures (MAT) are correlated to the distribution of the precipitation, with an overall correlation with elevation. At low elevation, we observe a general warming trend from west to east to the north and relatively homogenous warm MAT in the southern Pyrenees (Fig. 2B). Temperature seasonality is higher in the southern and in the northeastern Pyrenees (~ 16-17 °C) than in the northwestern and central northern Pyrenees

198 (12-14 °C) (Fig. 2C). This likely highlights the diversity of local climatology across this
199 range, ranging from oceanic to sub-continental to Mediterranean from west to east.
200 Oxygen isotope values are available from three GNIP (Global Network of Isotopes in
201 Precipitation, http://www.iaea.org/water) stations at low elevation in the northern Pyrenees.
202 One station located close to the Atlantic coastline (Dax) documents weighted mean annual
203 $\delta^{18}O$ of -5.4‰ and weighted mean annual δD of -31.9‰. A second one from the central
204 Pyrenees, at the foot of the main topographic relief at the head of the Lannemezan alluvial fan
205 (Campistrous), yields mean annual $\delta^{18}O$ and δD of -7.5‰ and – 46.3‰ respectively. Another
206 one in Toulouse yields $\delta^{18}O$ of -6.3‰ and δD of -38.8‰ (Fig. 1, Supplementary data 1).
207 GNIP stations from northern Spain are located relatively far from the Pyrenees, in the South-
208 Pyrenean foreland (Zaragoza, $\delta^{18}O$ = -5.7‰ and δD = -40.1‰), in Barcelona ($\delta^{18}O$ = -4.74‰
209 and δD = -26.8‰) on the Mediterranean coast and in Girona ($\delta^{18}O$ = -5.2‰ and δD = -
210 34.4‰). Correlation between isotopic values and climatic parameters at each station indicates
211 that $\delta^{18}O$ and δD are mostly correlated with seasonal temperature variations rather than with
212 the amount of precipitation (Supplementary data 1).
213
214
215 **4. Material and method**
216
217 Several sampling strategies are possible to document a topographic effect on the
218 isotopic composition of precipitation and rivers. The most obvious way is a direct monitoring
219 of rain at different locations and at various elevations. However, this approach presents some
220 logistical limitations because it requires a large network of stations all around the range, with
221 regular and synchronous samplings.

Isotopes vs. elevation investigations are therefore traditionally performed on rivers and streams at different elevations (Schemmel et al., 2013; Bershaw et al., 2016; Li and Garzione, 2016). This approach presents many advantages, because it allows a wide and representative sampling all over the mountain range. Moreover, during the dry season, groundwaters dominates the budget of small rivers and streams that correspond to a mix of the yearly rain, representing an annual mean of the isotopic composition of rain (Ingraham and Taylor, 1991; Schemmel et al., 2013). This allows avoiding the influence of transient climatic events on the isotopic composition of rivers, during which isotope/temperature data might not be correlated (Celle et al., 2000). The counterpart is that river and stream waters correspond to a mix of all rainfalls precipitated in the catchment above the sampling point and it is important to study small ones to avoid uncertainties related to the integration of a large elevation range (Poage and Chamberlain, 2001). We avoid sampling spring waters because of the lack of accuracy regarding the elevation at which rain effectively fell above the resurgence (Schemmel et al., 2013).

We have sampled 82 rivers and streams in the whole Pyrenees (Fig. 1A). They are draining ten main valleys in France, Spain and Andorra. More samples from the northern Pyrenees were collected due to the asymmetric distribution of precipitation and aridity between the two sides (Fig. 2). Thus, from west to east, we have sampled five main transects across the range. First, in the Basque Country, profile A-C begins near sea level south of Biarritz and crosses the divide at the Ronceveaux pass (B). It continues to the southwest and ends near the city of Pamplona (C). The second profile (D-F) is continuous from Pau to Huesca with a maximum elevation (~ 1750 m) at the Pourtalet pass (E). Stream and rivers were sampled in tributaries along the Ossau valley in France and along the Rio Gallego and Rio Isuela valleys in Spain. Six samples come from Navarre, between profiles B-C and E-F and are not integrated in any profile. The third profile (G-I) begins in France on the slope of

247 the Lannemezan alluvial fan and continues to the mains reliefs though the Neste d'Aure
248 valley up to its source (H). The profile continues to the south along the Rio Noguera
249 Ribagorçana and Noguera Pallaresa valleys (H'-I) in the Tremp Basin. Only four points could
250 be sampled in this area due to the elevated aridity. The fourth profile (J-L) begins to the south
251 of Toulouse, with samples have been collected in tributaries along the Ariège valley up to the
252 highest samples from Andorra (K; ~ 2100 m). The profile continues through the Cerdanya
253 Basin and the Sierra de Cadi to the south. The last profile (M-N) is oriented W-E and begins
254 at the top of the Têt valley. Samples come from small tributaries of the Têt River and finishes
255 south of Perpignan in the Roussillon Plain, near sea level.
256 Water was sampled during the dry season, from July to September, in summers 2013
257 to 2015, at least one week after the last rain, to minimize the effect of recent climatic events.
258 For each sample, 20 ml of water were collected and conditioned at low temperature to avoid
259 fractionation effects caused by evaporation.
260 Analyses were performed at the Institut d'Ecologie et des Sciences de
261 l'Environnement de Paris at Grignon. $\delta^{18}O$ analyses were performed by CO_2-H_2O
262 equilibration (Epstein and Mayeda, 1953) using isotope ratio mass spectrometer coupled to an
263 Aquaprep (Isoprime coupled to a Gilson X222, Micromass; standard error: 0.15 ‰). δD
264 measurements were produced by pyrolysis of the water molecule on a chrome reactor, with
265 continuous flow of ultra-pure helium using an isotope mass spectrometer PyrOH (Isoprime
266 coupled to an elemental analyzer EuroVector, Micromass; standard error: 0.8 ‰) (Morrison et
267 al., 2001). Oxygen and hydrogen isotopic measurements were expressed in "δ" notation.
268
269
270 **5. Results**
271

Results are summarized in Fig. 3, in which the spatial distribution of $\delta^{18}O$ and δD of streams and rivers around the Pyrenees is presented. The dependence on elevation is the same for the two isotopic ratios. The highest values are observed at low elevation whereas the ratios drop to negative values at high elevation. $\delta^{18}O$ ranges from -5.5 ‰ to -12.1 ‰ in the northern Pyrenees and from -6.5 ‰ to -11.1 ‰ in the southern Pyrenees. δD values range from -27.7 ‰ to -84.1 ‰ in the north and from -42.8 ‰ to -76.9 ‰ in the south. Figures 3B and 3D show the $\delta^{18}O$ and δD isotopic composition of river waters projected onto a topographic profile perpendicular to the central Pyrenees. Despite the apparent scattering of isotopic values with elevation, reflecting the variability of $\delta^{18}O$ and δD along the strike of the range, the figure shows that the northern side of the Pyrenees displays an isotope vs. elevation relationship that is not so clearly seen in the southern Pyrenees, especially at low elevation (Fig. 3B and 3D).

Plotting our $\delta^{18}O$ and δD data for each area, valley by valley, the dependence of isotopic ratios relative to elevation appears more clearly (Fig. 4 and 5). To the west (profile A-C), near sea-level values for the French Basque Country range between -5.7 and -6.3‰ for $\delta^{18}O$ and -27.7 and -31.9‰ for δD. Dependence on elevation is well documented for the French side, with a decrease of the isotopic ratios above the Ronceveaux pass at 1230 m (-9.3‰ for the $\delta^{18}O$ and -53.1‰ for the δD). In contrast, $\delta^{18}O$ and δD values are relatively constant in the southern side (B-C) and even decrease with elevation. On profile D-F, minimum values are reached at the Pourtalet pass (-11 ‰ and -75.4 ‰ for $\delta^{18}O$ and δD respectively). In this profile, we observe a decrease of $\delta^{18}O$ and δD with elevation on both sides of the range. A local decrease of isotopic ratios on top of the Sierra Exteriores is resolved in the southern Pyrenees. On profile G-H, a strong decrease of isotopic composition is measured from 220-280 m near the Lannemezan alluvial fan (~ -7 ‰ for $\delta^{18}O$ and ~ -65 ‰ for δD) to elevation of ~ 1800 m at Piau Engaly (-12.1 ‰ the $\delta^{18}O$ and -83.5 ‰ for δD). The

297 scattering of isotopic compositions of waters is more significant on profile H-I, so correlations
298 between elevation and $\delta^{18}O$ and δD appear less clear. On profile J-L, the highest $\delta^{18}O$ (-7.5
299 ‰) and δD (-49 ‰) are observed at the lowest elevation (~ 300 m) for the northern Pyrenees
300 and the most negative $\delta^{18}O$ (-11.9 ‰) and δD (-82.4 ‰) at 1800-2300 m in Andorra. Values
301 increase to the south in the Cerdanya Basin and through the Sierra de Cadi and the northern
302 Ebro Basin to reach -6.8 ‰ ($\delta^{18}O$) and -42.8 ‰ (δD) at 1100 m. Isotopic compositions along
303 the Têt valley (M-N profile) are well correlated with elevation from 1725 m (-11.7 ‰ for
304 $\delta^{18}O$ and -85.4 ‰ for δD) to the coast (max. $\delta^{18}O$ = -5.5 ‰ and δD = -38.8 ‰). Thus, the
305 near sea-level samples of the two northern terminations of the range have similar $\delta^{18}O$ values,
306 whereas δD is slightly more negative to the east. The decrease in isotopic composition with
307 elevation is obvious on the whole northern side of the range and is less clear in some profiles
308 in the southern Pyrenees.
309
310
311 **6. Discussion**
312
313 *6.1. Significance of the spatial distribution of the isotopic values*
314
315 To determine the moisture origin and to identify a possible recycling effect caused by
316 the evaporation of a surface water reservoir or during rainfall, we have calculated the
317 deuterium excess parameter (d) (Daansgard, 1964; Merlivat and Jouzel, 1979) (Fig. 6). This
318 parameter links the $\delta^{18}O$ and δD of water ($d = \delta D - 8 \times \delta^{18}O$). It can be considered as an
319 index of deviation from the Global Meteoric Water Line (GMWL), which is characterized by
320 a d-excess value of 10 ‰. d-excess is a parameter sensitive to the initial conditions during
321 evaporation from the ocean surface and is therefore a function of both temperature and

322 relative humidity at the oceanic source, as well as the speed of the wind and resistivity to
323 liquid – vapour transfer via a kinetic isotopic fractionation (Merlivat and Jouzel, 1979;
324 Froehlich et al., 2001). It is also a function of the conditions during the transport of moist air
325 and/or mixing of different air masses before moisture is condensed to form rainfall (Froehlich
326 et al., 2001). The general pattern is that d-excess in precipitation increases in response to
327 enhanced moisture recycling as a result of increased evaporate content. On the contrary, d-
328 excess is low when water is lost from air masses or rainfall due to evaporation (Froehlich et
329 al., 2001).

330 In the Pyrenees, the calculation of d-excess allows the identification of four different
331 water populations, characterized by distinct d-excess values (Fig. 6). First, in the northwestern
332 Pyrenees (profiles A-B and D-E, Fig. 1) d-excess is high and ranges from 15 ‰ to 22 ‰. The
333 central northern Pyrenees (G-H and J-K, Fig. 1) have intermediate d-excess values, between 7
334 and 14 ‰, whereas French Catalonia (M-N) have the lowest d-excess values, ranging from 3
335 ‰ to 11 ‰. In Spain, d-excess values are more homogenous and range from 7 ‰ to 14 ‰.

336 Considering back trajectory analysis, the mains sources of moisture in the Pyrenees
337 are the northern Atlantic Ocean and, at a lower proportion the Mediterranean Sea (Fig. 1). A
338 value of d ~ 10 ‰ is generally considered for moisture coming from the Atlantic Ocean to
339 southwestern Europe (Lambs et al., 2003) whereas the western Mediterranean Sea has a rather
340 higher d-excess (~ 14 ‰) due to its closed configuration (Celle et al., 2000). French GNIP
341 stations show higher mean annual weighted d-excess values than their Atlantic Ocean source
342 and lower than the western Mediterranean one, evolving from 11.3 ‰ at Dax to 13.4 ‰ at
343 Campistrous and to 11.8 ‰ at Toulouse (Supplementary data 1). River waters sampled at low
344 elevation also have high d-excess (~ 18 to 19 ‰) near the French Atlantic coast (A-B) and in
345 the Ossau Valley (D-E), and decrease in the central Pyrenees to 10 – 13 ‰ (G-H and J-K).
346 This pattern could reflect a possible mixing between Atlantic and Mediterranean moisture, but

347 the latter is supposed to have an influence only on the eastern coastline (Lambs et al., 2003).
348 HYSPLIT back trajectory analysis confirms that the north Atlantic Ocean is the main source
349 of moisture in the northwestern Pyrenees. Then, the high d-excess values of rain and rivers of
350 the northwestern Pyrenees are likely the expression of local surface water recycling
351 (Froehlich et al., 2001). The northwestern Pyrenees are also the location where MAP is the
352 highest at low elevation, so that these high d-excess values could also reflect the influence of
353 the amount effect (Lee and Fung, 2008; Botsyun et al., 2016).

354 It is worth noting that d-excess may show strong seasonal variations, such as seen at
355 the GNIP station of Dax between winter (d = ~15 ‰) and summer (d = ~3 ‰) due to colder
356 and less humid air masses during winter in the north Atlantic (Gonfiantini et al., 2001). Yet,
357 rainfall amounts and air temperatures exhibit strong seasonal variations, with maximal
358 precipitation and minimal temperatures being observed during winter and spring. It is likely
359 that the isotopic composition of the weighted mean annual values of rain at the three GNIP
360 stations and those of the Pyrenean rivers represent winter and spring values in majority, due to
361 this seasonally contrasted amount of rain and temperatures. We observe, however, that
362 monthly isotopic compositions of rain always present a better correlation with temperature
363 than precipitation values (Supplementary data 1).

364 Isotopic values of rivers at low elevation in northwestern and central northern
365 Pyrenees are also lower compared to values at the GNIP stations, with a difference of 0.5 to
366 1.5 ‰ and 1.5 to 12 ‰ for $\delta^{18}O$ and δD respectively (Fig. 6). The difference could reflect
367 isotopic fractionation in rain feeding rivers versus rain directly sampled at the stations.
368 However, it is important to determine what the water sampled in the Pyrenean rivers do
369 represent compared to rain. In the northwestern and central northern Pyrenees, the isotopic
370 composition of rain exhibits strong seasonal variations at the GNIP stations of Dax (from -2.3
371 ‰ to -6.8 ‰ for $\delta^{18}O$ and -14.5 ‰ to -45.8 ‰ for δD), Campistrous (from -3.2 ‰ to -9.8 ‰

372 for $\delta^{18}O$ and -15.2 ‰ to -66 ‰ for δD) and Toulouse (from -4.5 ‰ to -10.2 ‰ for $\delta^{18}O$ and -
373 24.8 ‰ to -71.8 ‰ for δD), with the most negative values recorded during winter
374 (Supplementary data 1). The amount of precipitation is also governed by seasonal cyclicities
375 and is the highest from October to May (Fig. 2).

376 On Fig. 7 we report the weighted mean and winter (from October to May) isotopic
377 values of rain at the GNIP stations of Dax, Campistrous and Toulouse and the isotopic
378 composition of rivers at low elevation located in the same area as these GNIP stations. Winter
379 isotopic values at GNIP stations shift to more negative values than the mean annual values
380 (Fig. 7). We also observe that GNIP winter and spring values are close to river samples at the
381 same elevation as the Campistrous GNIP Station. $\delta^{18}O$ and δD of rain remain slightly higher
382 at Toulouse for the low elevation samples from the Ariège valley, but these last ones were
383 sampled at mean elevation ~200 m higher than the Toulouse station. If we consider a mean
384 elevation effect of –0.28 ‰/100 m for $\delta^{18}O$ and –2.2 ‰/100 m for δD, as observed in many
385 other orogens (Rowley and Garzione, 2007), the weighted mean winter isotopic values of rain
386 at Toulouse fit with the low elevation samples of the Ariège valley (Fig. 7). Concerning the
387 French Basque Country (A-B), winter values at Dax are closer for $\delta^{18}O$, but remain different
388 for δD. This difference highlights that our river samples rather reflect winter and spring
389 isotopic values of rain than a mean of the annual values. It also illustrates that the effect of
390 moisture recycling is limited to the border of the Pyrenean range and that it is attenuated away
391 from the mains reliefs like at Dax.

392 In French Catalonia (profile M-N), d-excess values at low elevation are very low (d =
393 ~ 3-5 ‰). Back trajectory analysis reveals that rainfalls in the area come from the northern
394 Atlantic Ocean and the western Mediterranean Sea. d-excess values in this area are
395 significantly lower than thoses of the northern Atlantic (d = 10 ‰) and the western
396 Mediterranean Sea (d = 14 ‰). This difference reflects the influence of evaporation processes

on rain that source the eastern Pyrenean rivers (Froehlich et al., 2001). However, in this part of the range, low d-excess values are only observed at low elevation, where the highest temperature and lower precipitation are recorded in the area (Fig. 2). d-excess values are higher in the upper part of the Têt valley (profile M-N), where MAT are lower and precipitation increases (Fig. 6). This suggests that northeastern Pyrenean river-waters sampled at low elevation probably experienced evaporation compared to rain precipitated at higher elevation, and are not fully representative of the initial isotopic compositions of rain. Indeed, these samples come from small rivers with very reduced flow. We will thus not consider these values further.

In the southern Pyrenees, d-excess is more homogenous and ranges from 7 to 14 ‰. We do not observe significant variations in the southwestern to southeastern Pyrenees that could suggest the possible influence of different moisture sources, as the origin of the moisture remains nearly the same (i.e. Atlantic Ocean and Mediterranean Sea) in the whole southern Pyrenees (Fig. 1E and 1F). Moreover, d-excess is variable even for samples at low elevation. River samples at low elevation are located too far from the Spanish GNIP stations to make a reliable comparison like in France, but we can see great discrepancies in first approach.

6.2. Meteoric water lines

We have calculated the Local Meteoric Water Lines (LMWL), by plotting δD against $\delta^{18}O$ values in Fig. 8. We see that all Pyrenean values exhibit a relatively good overall correlation, with a small shift above the Global Meteoric Water Line (GMWL), but a similar slope (~ 8) (Fig. 8A). We also present a separate plot four distinct isotopic provinces based on

d-excess values (Fig. 8B). Outliers reveal the existence of four isotopic provinces that exhibit distinct isotopic characteristics, and that give three LMWL for the northern Pyrenees and one for the south:

$$\text{Northwestern Pyrenees: } \delta D = 7.67\ \delta^{18}O + 15.47 \quad (1)$$

$$\text{Central northern Pyrenees: } \delta D = 7.79\ \delta^{18}O + 9.82 \quad (2)$$

$$\text{Northeastern Pyrenees: } \delta D = 8.15\ \delta^{18}O + 10.12 \quad (3)$$

The northwestern Pyrenees present the most distinct values (eq. 1; Fig. 8B). The correlation line is the most shifted, but the slope is close to the GMWL. The central northern Pyrenees follow the same tendency, with a shift to values closer to the GMWL (eq. 2). After the removal of values at low elevation with very low d-excess, the northeastern Pyrenees exhibit a relationship that is very close to the GMWL (eq. 3). It is also close to the relationship determined by Celle et al. (2000) for the station of Avignon in southern France.

We also plotted isotopic compositions of rivers against MAP and MAT, extracted for each sampling area from the data of Hijmans et al. (2005) (Fig. 8C to 8F). We observe that the isotopic compositions of the northwestern Pyrenean rivers are poorly correlated with MAP (R^2 of 0.06 and 0.05 for $\delta^{18}O$ and δD respectively), contrary to MAT (R^2 of 0.8 for $\delta^{18}O$ and δD). On the contrary, central northern and northeastern Pyrenees exhibit good correlations with both MAP and MAT (R^2 comprised between 0.7 and 0.85).

The good agreement of these three LMWL with the GMWL shows that river waters reflect regional precipitation and that the evaporation effect is small. We conclude that the isotopic composition of rain and rivers in the northern Pyrenees results principally from

447 temperature variations and thus from the altitudinal effect. This suggests that the Pyrenees are
448 high enough to exert an orographic effect on the isotopic composition of rain and rivers.
449
450 The Spanish Pyrenees show the lowest slope that cuts the GMWL:
451
452 Southern Pyrenees: $\delta D = 7.26\ \delta^{18}O + 3.89$ (4)
453
454 The slope measured for the southern Pyrenean LMWL is the lowest of the four
455 isotopic provinces around the Pyrenees, but it remains close to the GMWL. This low slope is
456 probably due to the evaporation of moisture during rain events as a consequence of higher
457 MAT and lower MAP on the southern side of the range compared to the northern side (Celle
458 et al., 2001). In this area, isotopic compositions of rivers show weak correlations with both
459 MAP and MAT (Fig. 8C to 8F).
460 The deviation from the GMWL remains limited however compared to highly elevated
461 mountain ranges where the slope of the LMWL in the true leeward side is > 6, like in the
462 Andes or the Central Anatolian Plateau (Gonfiantini et al., 2001; Schemmel et al., 2013).
463 Thus, the southern Pyrenees cannot be considered as a true leeward side influenced by a real
464 rain shadow effect.
465 We can define several processes from these four LMWL. The first orographic
466 precipitation from the northern Atlantic source falls over the whole northwestern Pyrenees,
467 and has relatively homogenous characteristics at least 150-200 km inland. Due to the
468 continentality effect, as moisture is translated to the central Pyrenees, the isotopic
469 composition of rain water follows a distinct LWML with a slope close to the GMWL that is
470 similar to the northwestern Pyrenees. This evolution can be considered as the result of the
471 continentality effect, as littoral domains receive rainwater corresponding to the firsts steps of

moisture condensation with enriched isotopic values. A similar slope between the two isotopic provinces shows that clouds migrate inland without suffering significant evaporation or water recycling. Back trajectory analysis indicates that the influence of the western Mediterranean Sea is proportionally more important in the northeastern Pyrenees (profile M-N) than in the northwestern and north central Pyrenees and represents a more equilibrated mix of the Atlantic and Mediterranean moisture sources (Fig. 1D). We note however that the contintentality effect is greater on the Atlantic source, which is still important for the origin of the rain arriving in the northeastern Pyrenees. The southern Pyrenees constitute an isotopically more isolated area compared to the north, where precipitation is lower and moisture more recycled to the atmosphere during rainfall events.

6.3. Isotopic lapse rate

Considering that elevation to first order drives the isotopic composition of rain in the French Pyrenees, we have calculated isotopic lapse rates for $\delta^{18}O$ and δD for the four studied isotopic provinces (Fig. 9). Modern isotopic lapse rates constitute a cornerstone for paleoelevation studies. As we sampled rivers and not directly rain, we need to apply a correction accounting for the mean basin hypsometry that corresponds to the average elevation of the watershed upstream from the sampling area (Poage and Chamberlain, 2001). This is why we have sampled river waters as high as possible in the watersheds. At the scale of the Pyrenees, we have calculated a mean difference of ~ 180 m between the sampling elevation of springs and rivers and the mean elevation of the corresponding watershed.

Results indicate that isotopic lapse rates differ for the four studied areas. The lowest lapse rates are measured in the northwestern Pyrenees (-2.6 and -21.4 ‰/km for $\delta^{18}O$ and δD

497 respectively). The central northern Pyrenees exhibit slightly higher isotopic lapse rates,
498 increasing strongly in the northeastern Pyrenees and passing from -2.8 to -3.8 ‰/km for $\delta^{18}O$
499 and -21.4 ‰/km to -31.7 ‰/km for δD. The isotopic values obtained in the French Pyrenees
500 are in good agreement with the global means of isotopic lapse rates recovered for the
501 windward sides of the main orogens, which are -2.8 ‰/km and -22 ‰/km for $\delta^{18}O$ and δD
502 respectively (Rowley and Garzione, 2007). Lapse rates are much higher on the Spanish side
503 of the Pyrenees (–9.5 ‰/km and –77.5 ‰/km), with a great scattering of isotopic data and a
504 very low coefficient of correlation. This result confirms that the elevation effect is not the
505 dominating factor on the isotopic composition of rain and rivers in that side of the range.
506 Therefore, reliable paleoelevation quantifications are difficult to obtain on the southern flank
507 of the Pyrenees.

508 We have also reported on Fig. 9 the mean annual and winter weighted isotopic values
509 of the GNIP stations. It appears that the Spanish GNIP stations are at odds with the lapse rate
510 from river samples on the southern side of the range. Concerning the French stations, mean
511 annual GNIP values are enriched compared to the river samples, except for deuterium in the
512 French Basque-Country. However, the mean weighted winter values are shifted to more
513 negative values, which better fits with the isotopic compositions of rivers. This finding
514 confirms that our samples reflect the mean of precipitation during winter and spring.

515

516

517 **7. Implications for paleotopographic reconstructions**

518

519 Figure 10 presents a comparison between the Pyrenees and the other main mountain
520 ranges where $\delta^{18}O$ vs elevation relationships have been investigated (Fig. 10). The figure
521 demonstrates that the northern side of the Pyrenees shows an isotopic lapse rate close to -2.8

522 ‰/km, in good agreement with other highly elevated mountain ranges of the world. Pyrenean
523 $\delta^{18}O$ values of rivers at low elevation are close to those of the northeastern Bolivian Plateau
524 and both the measured river and modelled precipitation of the south central Himalaya (~ -7 to
525 -6 ‰; Garzione et al., 2000; Rowley et al., 2001). In Europe, values at low elevation from the
526 northern Pyrenees are slightly more positive, but close to the published values from the
527 southern Alps (Schotterer et al., 1997) and the Pontic Montains (Northern Central Anatolian
528 Plateau; Schemmel et al., 2013).

529 Our results imply that, despite their relatively low elevation, the Pyrenees exhibit the
530 classical features of highly elevated mountains ranges. First, they are characterized by a
531 distinct northern side, where precipitation dominates compared to evaporation and where the
532 altitudinal effect is the main parameter controlling the isotopic composition of rain and rivers.
533 However, on the southern side, elevation is not the only parameter controlling isotopic
534 composition of rivers. A probable control by evaporation during rainfall, or of surface
535 moisture, appears to hinder reliable estimates of the altitudinal effect on isotopic composition
536 of precipitation. Our study shows that the Pyrenees constitute a promising site for the
537 investigation of paleoaltitudes, and the establishment of arid conditions on its southern flank
538 through isotopic approaches.

539 However, the geographic and climatic features of the Pyrenees introduce specific
540 biases that are important to consider for paleoaltitude investigations. In particular, the
541 orientation of the main topography is parallel to the main wind trajectory and orthogonal to
542 the coasts. Two main sources of moisture are reported on both sides of the range on the
543 northern side. In addition, the effect of continentality and mixing of these distinct moisture
544 sources is reflected along the strike of the orogen in the differences in isotopic lapse rate of ~
545 1 ‰/km and ~ -10 ‰/km for $\delta^{18}O$ and δD respectively.

546

8. Conclusion

We have demonstrated that, despite their relative low elevation and size compared to other ranges like the Andes, the Sierra Nevada or the Himalaya, the Pyrenees exert an orographic effect on precipitation and isotopic composition of rain and rivers. The two sides can be distinguished according to their climatic and isotopic signatures. To the north, precipitation dominates compared to evaporation, and the altitudinal effect is the main driver of the $\delta^{18}O$ and δD composition of rain. To the south, precipitation is lower at low elevation. As a consequence, moisture is more recycled and the altitudinal effect and amount effects are not the only parameters controling the isotopic composition of rain. No reliable paleoaltitudinal reconstructions are therefore possible on this side of the orogen. A significant lateral isotopic gradient is documented from west to east due to a combination of the continentality effect and the influence of two moisture sources. As a consequence, local lapse rates have to be taken into account depending on the area considered along the strike of the orogen. These new results provide critical constraints for future investigations of past elevation reconstructions of small mountain ranges using stable isotopic geochemistry.

Acknowledgements

We would like to thank Christelle Arduini, Nicolas Beaudoin and Franck Lartaud for their help on the field and Xavier Lalande for is help on Qgis. This work is a contribution to ANR PYRAMID Project. Editor Derek Vance, Svetlana Botsyun and an anonymous reviewer are thanked for their fruitful comments that improved the manuscript.

572 **Figure captions**

573

574 **Figure 1**: A: Location of samples analyzed in this study and GNIP Stations. Samples with
575 white circles are the rivers at low elevation compared to the three French GNIP stations in
576 Figure 7. HYSPLIT back trajectories analyses are presented for five areas around the
577 Pyrenees, indicating the origin of the moisture up to 72h before its arrival. Back trajectories
578 end points are located B: in the northwestern C: in the northern central D: in the northeastern,
579 E: in the south central and F: in the southeastern Pyrenees respectively.

580

581 **Figure 2**: A: mean annual precipitation and B: mean annual temperature around the Pyrenees
582 (from Hijmans et al., 2005). C: mean monthly temperature and precipitation from GNIP
583 stations for Campistrous, Toulouse, Perpignan and Girona, from Météo France for Biarritz
584 and from the State Meteorological Agency (AEMET) of Spain for Pamplona and Huesca.

585

586 **Figure 3**: A: $\delta^{18}O$ values of small rivers and streams sampled around the Pyrenees. B:
587 projection of $\delta^{18}O$ values along a topographic cross section in the central Pyrenees. C: δD
588 values of small rivers and streams sampled around the Pyrenees. D: projection of δD values
589 along a topographic cross section in the central Pyrenees.

590

591 **Figure 4**: Distribution of $\delta^{18}O$ values of small rivers and streams in each valley sampled
592 around the Pyrenees (except the Navarre area). Mean annual temperature and precipitation
593 profiles are reported for each area (from Hijmans et al., 2005). Mean annual weighted value
594 for the Campistrous GNIP station is reported in the Lannemezan – Aure valley profile (G-H).

595

Figure 5: Distribution of δD values of small rivers and streams in each valley sampled around the Pyrenees (except the Navarre area). Mean annual temperature and precipitation profiles are reported for each area (from Hijmans et al., 2005). Mean annual weighted value for the Campistrous GNIP station is reported in the Lannemezan – Aure valley profile (G-H).

Figure 6: Distribution of the deuterium excess parameter (d) for rivers and streams around the Pyrenees. The differences in d-excess values in each valley allow the identification of four main isotopic provinces around the Pyrenees: northwestern, central northern, northeastern and southern Pyrenees.

Figure 7: Plot of $\delta^{18}O$ vs. δD values for the French Basque-Country, Lannemezan and Ariège valley at low elevation and the mean annual and winter (October to April) weighted values of the Dax, Campistrous and Toulouse GNIP stations. IThe isotopic composition of rivers mostly reflects the isotopic composition of rain precipitate during the winter season. The Global Meteoric Water Line (GMWL) is also reported. River samples at low elevation are located in Fig. 1 for each sector.

Figure 8: Meteoric water lines (δD vs $\delta^{18}O$ relationships) of all water samples from the whole Pyrenees (A) and separately for each isotopic province in the northern and southern Pyrenees (B) as done using deuterium excess values. The Global Meteoric Water Line (GMWL) is also reported. C and D: plot of $\delta^{18}O$ and δD values against mean annual precipitation values at the sampling point, extracted from Fig. 2A. E and F: plot of $\delta^{18}O$ and δD values against mean annual temperature at the sampling point, extracted from Fig. 2B.

Figure 9: Isotopic lapse rates for the four isotopic provinces. Elevation corresponds to the mean elevation in the watershed upstream of the sampling site. Mean annual and winter (October to May) values of the French GNIP stations are also reported.

Figure 10: Modern $\delta^{18}O$ isotopic lapse rates from rain or surface water measurements for the main studied mountain ranges of the world illustrating the isotopic variability according to the initial isotopic composition of the moisture source. The calculated lapse rates for the French Pyrenees are also reported, showing good correspondance with the most elevated mountain ranges.

Supplementary data 1: Climatic and isotopic data of the GNIP stations around the Pyrenees in France and Spain (IAEA/WMO, 2017). Data for Toulouse are from Lamb et al., 2013. Winter values are calculated from monthly data of each station from October to May, weighted from the amount of precipitation.

Supplementary data 2: Isotopic composition and location of the river-water sampled in this study.

638 **References:**

639

640 Allen, P., 2008. From landscapes into geological history. Nature 451, 274-276.

641 Araguas-Araguas, L.J., Diaz Teijeiro, M.F., 2005. Isotope composition of precipitation and
642 water vapour in the Iberian Peninsula. In: Isotopic composition of precipitation in the
643 Mediterranean Basin in relation to air circulation patterns and climate. International
644 Atomic Energy Agency-Isotopic composition of precipitation in the Mediterranean
645 Basin in relation to air circulation patterns and climate. International Atomic Energy
646 Agency, 173-190.

647 Babault, J., Van Den Driessche, J., Bonnet, S., Castelltort, S., Crave, A., 2005. Origin of the
648 highly elevated Pyrenean peneplain. Tectonics 24, TC2010.

649 Bershaw, J., Saylor, J.E., Garzione, C.N., Leier, A., Sundell, K.E., 2016. Stable isotope
650 variations ($\delta^{18}O$ and δD) in modern waters across the Andean Plateau. Geochimica et
651 Cosmochimica Acta 194, 310-324.

652 Botsyun, S., Sepulchre, P., Risi, C., Donnadieu, Y., 2016. Impacts of Tibetan Plateau uplift on
653 atmospheric dynamics and associated precipitation $\delta^{18}O$. Climate of the Past 12(6),
654 1401-1420.

655 Campani, M., Mulch, A., Kempf, O., Schlunegger, F., Mancktelow, N., 2012. Miocene
656 paleotopography of the Central Alps. Earth and Planetary Science Letters 337-338, 174-
657 185.

658 Caves, J., Winnick, M.J., Graham, S.A., Sjostrom, D.J., Mulch, A., Chamberlain, C.P., 2015.
659 Roel of the westerlies in Central Asia climate over the Cenozoic. Earth and Planetary
660 Science Letters 428, 33-43.

661 Celle, H., Daniel, M., Mudry, J., Blavoux, B., 2000. Signal pluie et traçage par les isotopes
662 stables en Méditerranée occidentale. Exemple de la région avignonnaise (Sud-Est de la
663 France). Comptes Rendus de l'Académie des Sciences-Series IIA-Earth and Planetary
664 Science 331(10), 647-650.

665 Celle-Jeanton, H., Travi, Y., Blavoux, B., 2001. Isotopic typology of the precipitation in the
666 Western Mediterranean region at three different time scales. Geophysical Research
667 Letters 28(7), 1215-1218.

668 Chen, F.-H., Yu, Z., Yang, M., Ito, E., Wang, S., Madsen, D.B., Huang, X., Zhao, Y., Sato,
669 T., Birks, H.J.B., Boomer, I., Chen, J., An, C., Wünnemann, B., 2008. Holocene
670 moisture evolution in arid central Asia and its out-of-phase relationship with Asian
671 monsoon history. Quaternary Science Reviews 27, 351–364.

672 Christophoul, F., Soula, J.-C., Brusset, S., Elibana, B., Roddaz, M., Bessiere, G., Deramond,
673 J., 2003. Time, place and mode of propagation of foreland basin systems as recorded by
674 the sedimentary fill: examples of the Late Cretaceous and Eocene retro-foreland basins
675 of the north-eastern Pyrenees. Geological Society, London, Special Publications 208,
676 229-252, doi:10.1144/GSL.SP.2003.208.01.11.

677 Dansgaard, W., 1964. Stable isotopes in precipitation. Tellus 16, 436-468.

678 Ehlers, T.A., Poulsen, C.J., 2009. Influence of Andean uplift on climate and paleoaltimetry
679 estimates. Earth and Planetary Science Letters 281 (3–4), 238–248.

680 Epstein, S., Mayeda, T., 1953. Variation of ^{18}O content of waters from natural sources.
681 Geochimica et Cosmochimica Acta 4, 213-224.

682 Filleaudeau, P.Y., Mouthereau, F., Pik, R, 2012. Thermo-tectonic evolution of the south-
683 central Pyrenees from rifting to orogeny: insights from detrital zircon U/Pb and (U-
684 Th)/He thermochronometry. Basin Research 24, 401-417.

685 Fons, M.C., 1979. Cyclogenèses du bassin méditerranéen occidental. Monographie n°109,
686 Météorologie Nationale.

687 Froehlich, K., Gibson, J. J., Aggarwal, P., 2001. Deuterium excess in precipitation and its
688 climatological significance. In Study of Environmental Change Using Isotope
689 Techniques. International Atomic Energy Agency, C&S Papers Series, 13, 54-66.

690 Garcia-Castellanos, D., Vergés, J., Gaspar-Escribano, J., Cloetingh, S., 2003. Interplay
691 between tectonics, climate, and fluvial transport during the Cenozoic evolution of the
692 Ebro Basin (NE Iberia). Journal of Geophysical Research 108 (B7), 2347, http://dx.doi.
693 org/10.1029/2002JB002073.

694 Garzione, C.N., Quade, J., DeCelles, P.G., English, N.B., 2000. Predicting paleoelevation of
695 Tibet and the Himalaya from $\delta^{18}O$ vs. altitude gradients in meteoric water across the
696 Nepal Himalaya. Earth and Planetary Science Letters 183, 215–229.

697 Garzione, C.N., Auerbach, D.J., Smith, J.J.S., Rosario, J.J., Passey, B.H., Jordan, T.E., Eiler,
698 J.M., 2014. Clumped isotope evidence for diachronous surface cooling of the Altiplano
699 and pulsed surface uplift of the Central Andes. Earth and Planetary Science Letters 393,
700 173-181.

701 Gébelin, A., Mulch, A., Teyssier, C., Jessup, M.J., Law, R.D., Brunel, M., 2013. The Miocene
702 elevation of Mount Everest. Geology 41, 799-802.

703 Gonfiantini, R., Roche, M.A., Olivry, J.C., Fontes, J.C., Zuppi, G.M., 2001. The altitude
704 effect on the isotopic composition of tropical rains. Chemical Geololgy 181, 147–167.

705 Gunnell, Y., Zeyen, H., Calvet, M., 2008. Geophysical evidence of a missing lithospheric root
706 beneath the eastern Pyrenees: consequences for post-orogenic uplift and associated
707 geomorphic signatures. Earth and Planetary Science Letters 276, 302–313.

Hijmans, R., Cameron, S.E., Parra, J.L., Jones, P.G., Jarvis, A., 2005. Very high resolution interpolated climate surfaces for global land areas. International Journal of Climatology 25, 1965-1978

Huyghe, D., Mouthereau, F., Castelltort, S., Filleaudeau, P-Y., Emmanuel, L., 2009. Paleogene propagation of the southern Pyrenean thrust wedge revealed by finite strain analysis in frontal thrust sheets: implications for mountain building, Earth and Planetary Science Letters 288, 421-433.

Huyghe, D., Mouthereau, F., Emmanuel, L., 2012a. Oxygen isotopes of marine mollusc shells record Eocene elevation change in the Pyrenees. Earth and Planetary Science Letters 345-348, 131-141.

Huyghe, D., Castelltort, S., Mouthereau, F., Serra-Kiel, J., Filleaudeau, P.-Y., Berthier, B., Emmanuel, L., Renard, M., 2012b. Large scale facies change in the middle Eocene South-Pyrenean foreland basin: The role of tectonics and prelude to Cenozoic ice-age. Sedimentary Geology 253-254, 25-46.

IAEA/WMO, 2017. Global Network of Isotopes in Precipitation. The GNIP Database. Accessible at: http://www.iaea.org/water

Ingraham, N.L., Taylor, B.E., 1991. Light stable isotope systematics of large-scale hydrologic regimes in California and Nevada. Water Resources Research 27, 77–90.

Insel, N., Poulsen, C.J., Ehlers, T.A., Sturn, C., 2012. Response of meteoric $\delta^{18}O$ to surface uplift – Implications for Cenozoic Andean Plateau growth. Earth and Planetary Science Letters 317-318, 262-272.

Lambs, L., Moussa, I., Brunet, F., 2013. Air masses origin and isotopic tracers: a study case of the oceanic and Mediterranean rainfall southwest of France. Water 5, 617-628. doi: 10.3390/w5020617.

732 Lee, J.E., Fung, I., 2008. “Amount effect” of water isotopes and quantitative analysis of
733 post- condensation processes. Hydrological Processes 22(1), 1-8.

734 Li, L., Garzione, C.N., 2017. Spatial distribution and controlling factors of stable isotopes in
735 meteoric waters on the Tibetan Plateau: Implications for paleoelevation
736 reconstruction. Earth and Planetary Science Letters 460, 302-314.

737 Longinelli, A., Selmo, E., 2003. Isotopic composition of precipitation in Italy: a first overall
738 map. Journal of Hydrology 270, 75–88.

739 Merlivat L., Jouzel J., 1979. Global climatic interpretation of the deuterium-oxygen 18
740 relationship for precipitation. Journal of Geophysical Research 84 (C8), 5029-5033.

741 Morrison, J., Brockwell, T., Merren, T., Fourel, F., Phillips, A.M., 2001. On-Line High-
742 Precision Stable Hydrogen Isotopic Analyses on Nanoliter Water Samples. Analytical
743 Chemistry 73(15), 3570-3575.

744 Mouthereau, F., Filleaudeau, P.-Y., Vacherat, A., Pik, R., Lacombe, O., Fellin, M.G.,
745 Castelltort, S., Christophoul, F., Masini, E., 2014. Placing limits to shortening evolution
746 in the Pyrenees: Role of margin architecture and implications for the Iberia/Europe
747 convergence. Tectonics 33, doi:10.1002/2014TC003663.

748 Mulch, A., 2016. Stable isotope paleoaltimetry and the evolution of landscapes and life. Earth
749 and Planetary Science Letters 433, 180-191.

750 Muñoz, J.A.E., 1992. Evolution of a continental collision belt: ECORS-Pyrenees crustal
751 balanced cross-section, in: K. McClay, (Ed), Thrust Tectonics, Chapman & Hall, pp.
752 235-246.

753 Poage, M.A., Chamberlain, P., 2001. Empirical relationships between elevation and the stable
754 isotope composition of precipitation and surface waters: considerations for studies of
755 paleoelevation change. American Journal of Science 301, 1-15.

Quade, J., Breecker, D.O., Daëron, M., Eiler, J., 2011. The paleoaltimetry of Tibet: an isotopic perspective. American Journal of Science 311, 77-115.

Rowley, D.B., Currie, B.S., 2006. Paleo-altimetry of the late Eocene to Miocene Lunpola basin, central Tibet. Nature 439, 677–681.

Rowley, D.B., Garzione, C., 2007. Stable-isotope based paleoaltimetry. Annual Review of Earth and Planetary Science 35, 463–506.

Rowley, D.B., Pierrehumbert, R.T., Currie, B.S., 2001. A new approach to stable isotope-based paleoaltimetry: implications for paleoaltimetry and paleohypsometry of the High Himalaya since the Late Miocene. Earth of Planetary Science Letters 188, 253–268.

Schemmel, F., Mikes, T., Rojay, B., Mulch, A., 2013. The impact of topography on isotopes in precipitation across the Central Anatolian Plateau (Turkey). American Journal of Science 313, 61–80.

Schotterer, U., Frohlich, K., Gaggeler, H.W., Sandjordj, S., Stichler, W., 1997. Isotope records from Mongolian and alpine ice cores as climate indicators. Climatic Change 36, 519–530.

Sinclair, H.D., Gibson, M., Naylor, M., Morris, G., 2005. Asymetric growth of the Pyrenees revealed through measurement and modeling of orogenic fluxes. American Journal of Science 305, 369-406.

Stein, A.F., Draxler, R.R, Rolph, G.D., Stunder, B.J.B., Cohen, M.D., Ngan, F., 2015. NOAA's HYSPLIT atmospheric transport and dispersion modeling system, Bulletin of the American Meteorological Society 96, 2059-2077, http://dx.doi.org/10.1175/BAMS-D-14-00110.1.

778 Suc, J.-P., Fauquette, S., 2012. The use of pollen floras as a tool to estimate palaeoaltitude of
779 mountains: The eastern Pyrenees in the Late Neogene, a case study. Palaeogeography,
780 Palaeoclimatology, Palaeoecology 321-322, 41-54.

781 Vacherat, A., Mouthereau, F., Pik, R., Huyghe, D., Paquette, J.-L., Christophoul, F., Loget,
782 N., Tibari, B., 2017 Rift-to-collision sediment routing in the Pyrenees: a synthesis from
783 sedimentological, geochronological and kinematic constraints. Earth-Science Reviews
784 172, 43-74.

785 Vergés, J., Fernandez, M., Martinez, A., 2002. The Pyrenean orogen: pre-, syn-, and post-
786 collisional evolution. In: Rosenbaum, G. and Lister, G. S. 2002. Reconstruction of the
787 evolution of the Alpine-Himalayan Orogen. Journal of the Virtual Explorer 8, 55 - 74.

788 Winnick, M.J., Welker, J.M., Chamberlain, C.P., 2014. Quantifying the isotopic "Continental
789 Effect". Earth and Planetary Science Letters 406, 123–133.

790

Figure-1

Click here to download Figure: Fig-1-carte ech-small.pdf

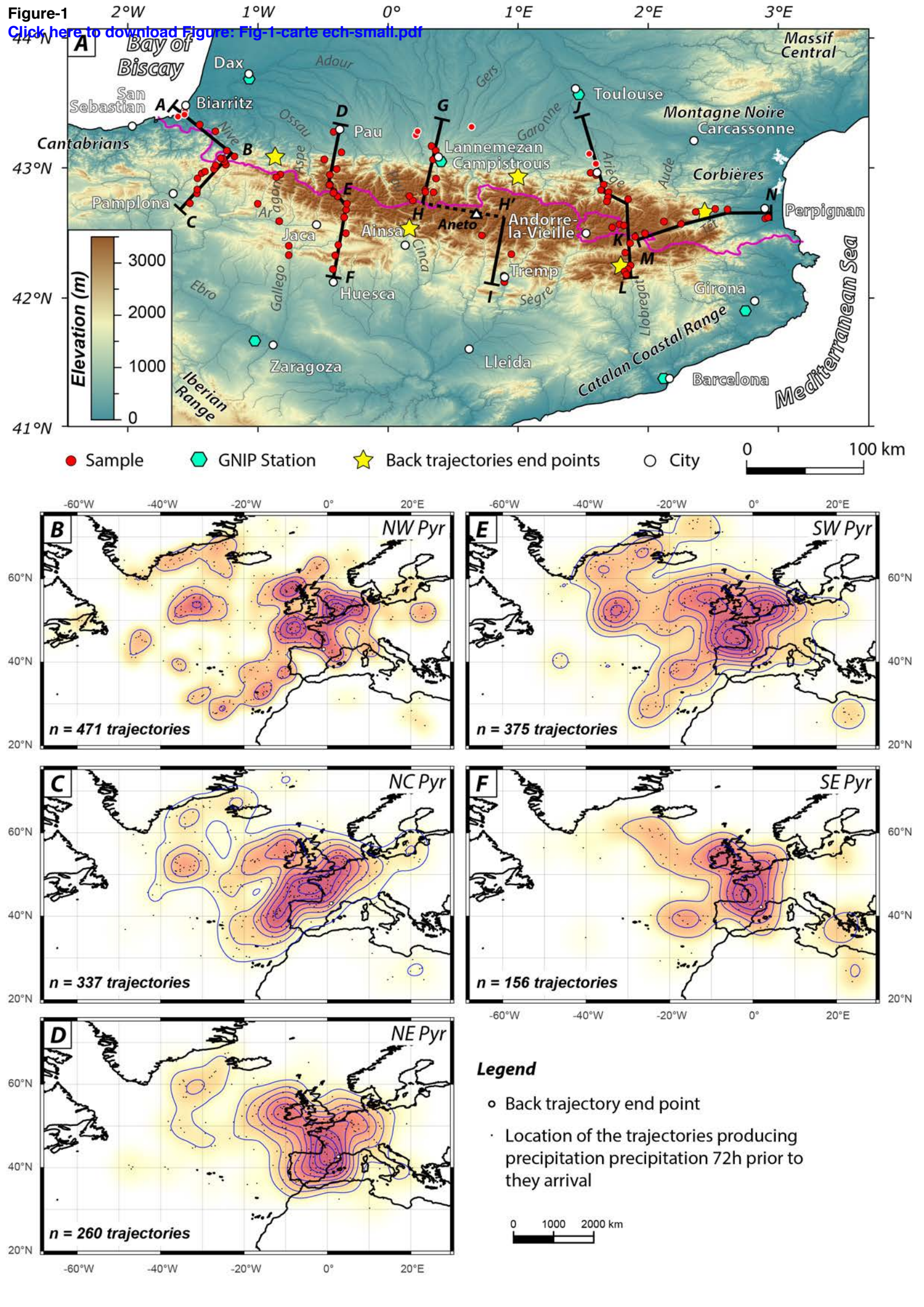

Figure-2

Click here to download Figure: Fig-2 MAT MAP V2-small.pdf

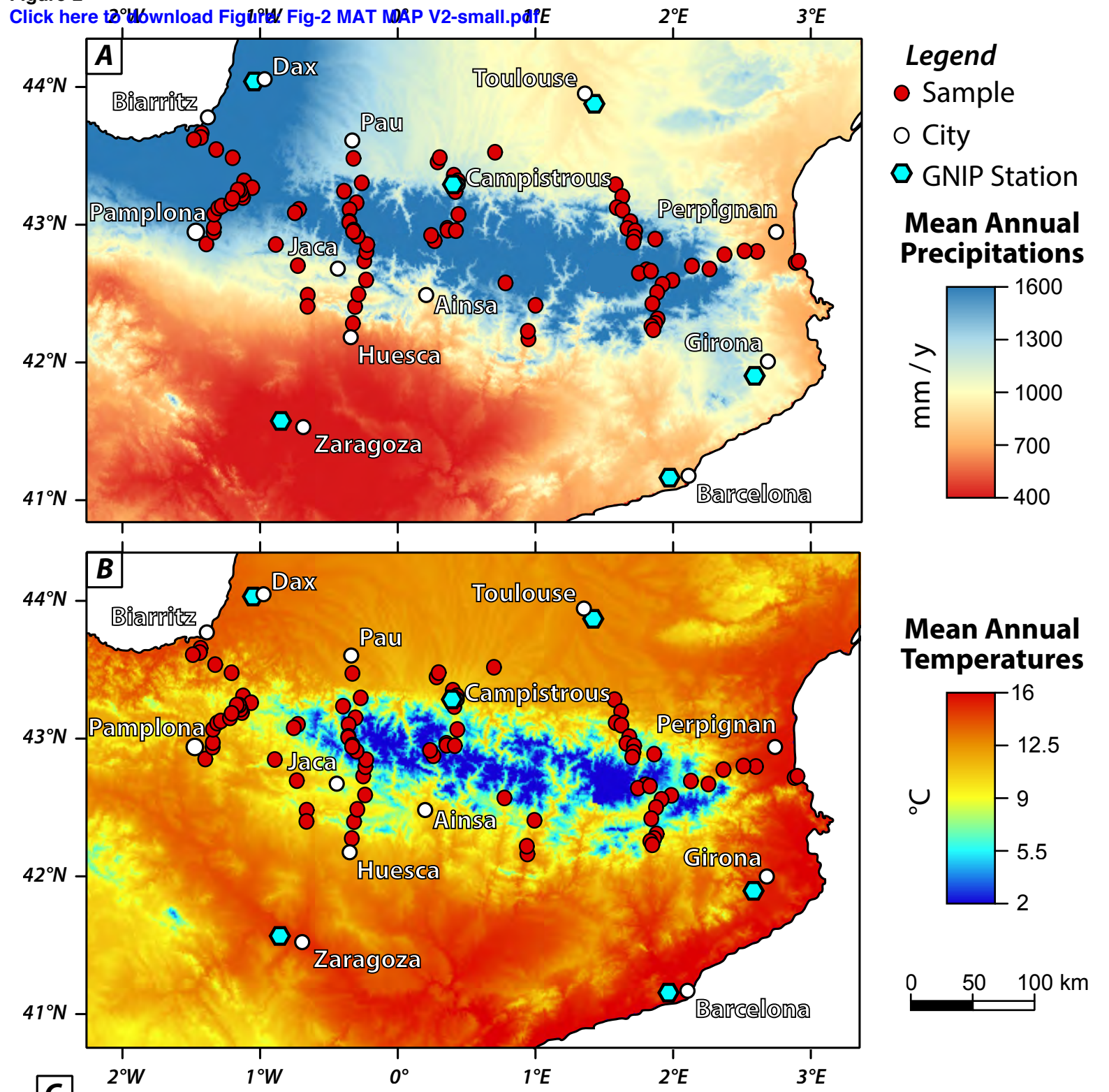

Figure-3

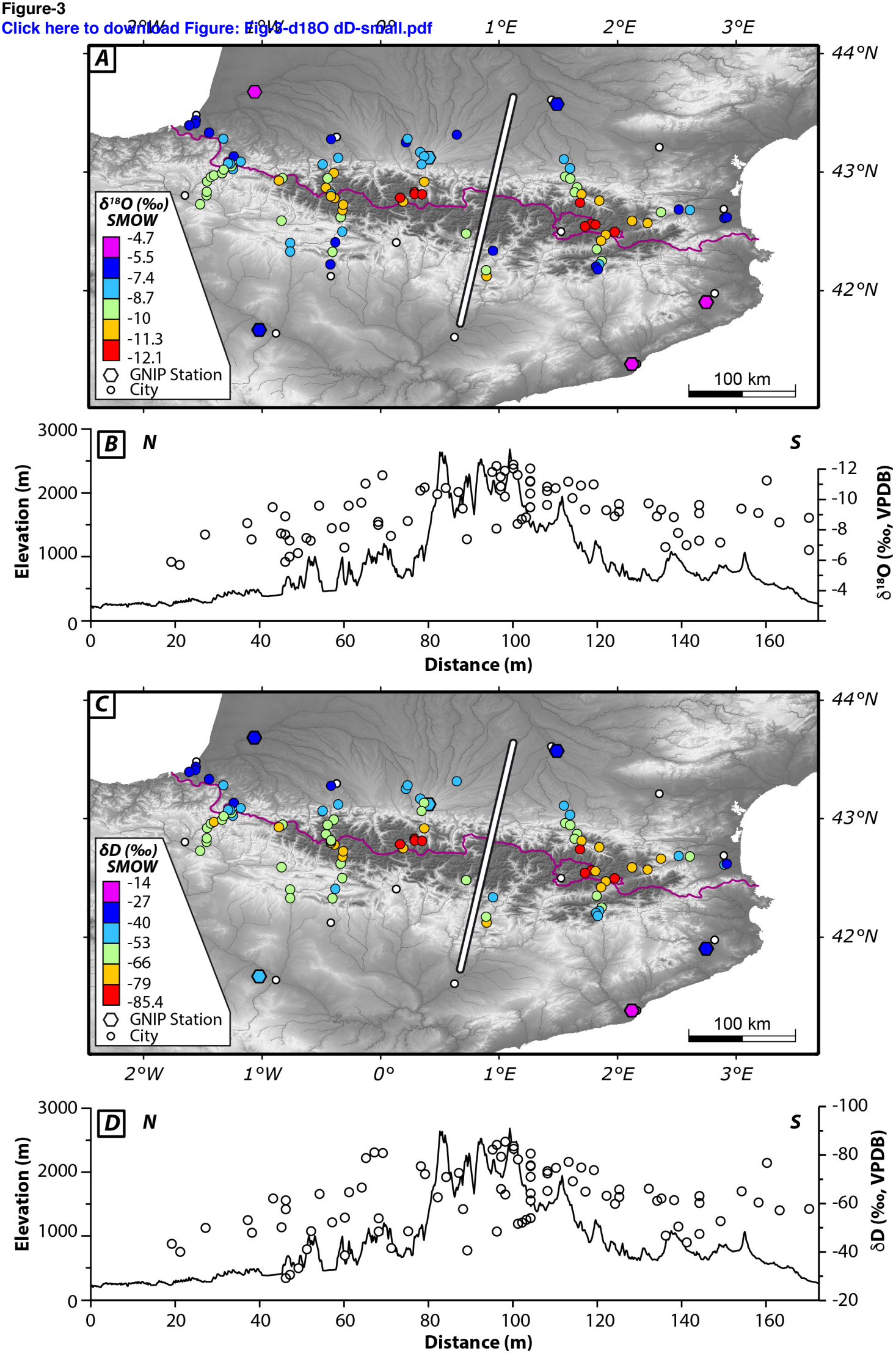

Figure-4

Click here to download Figure: Fig-4-profiled18O.pdf

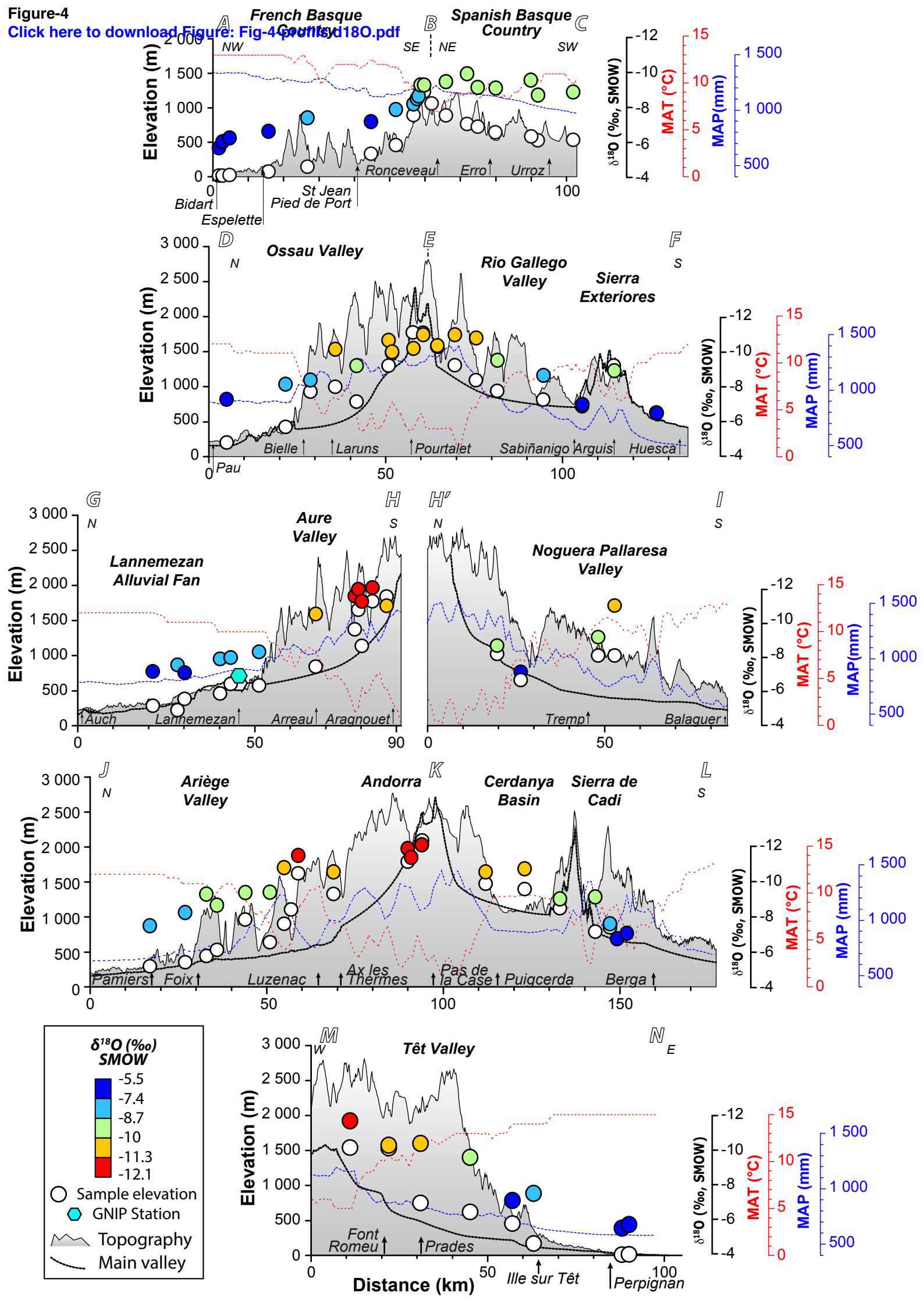

Figure-5

Click here to download Figure: Fig-5-profilesD.pdf

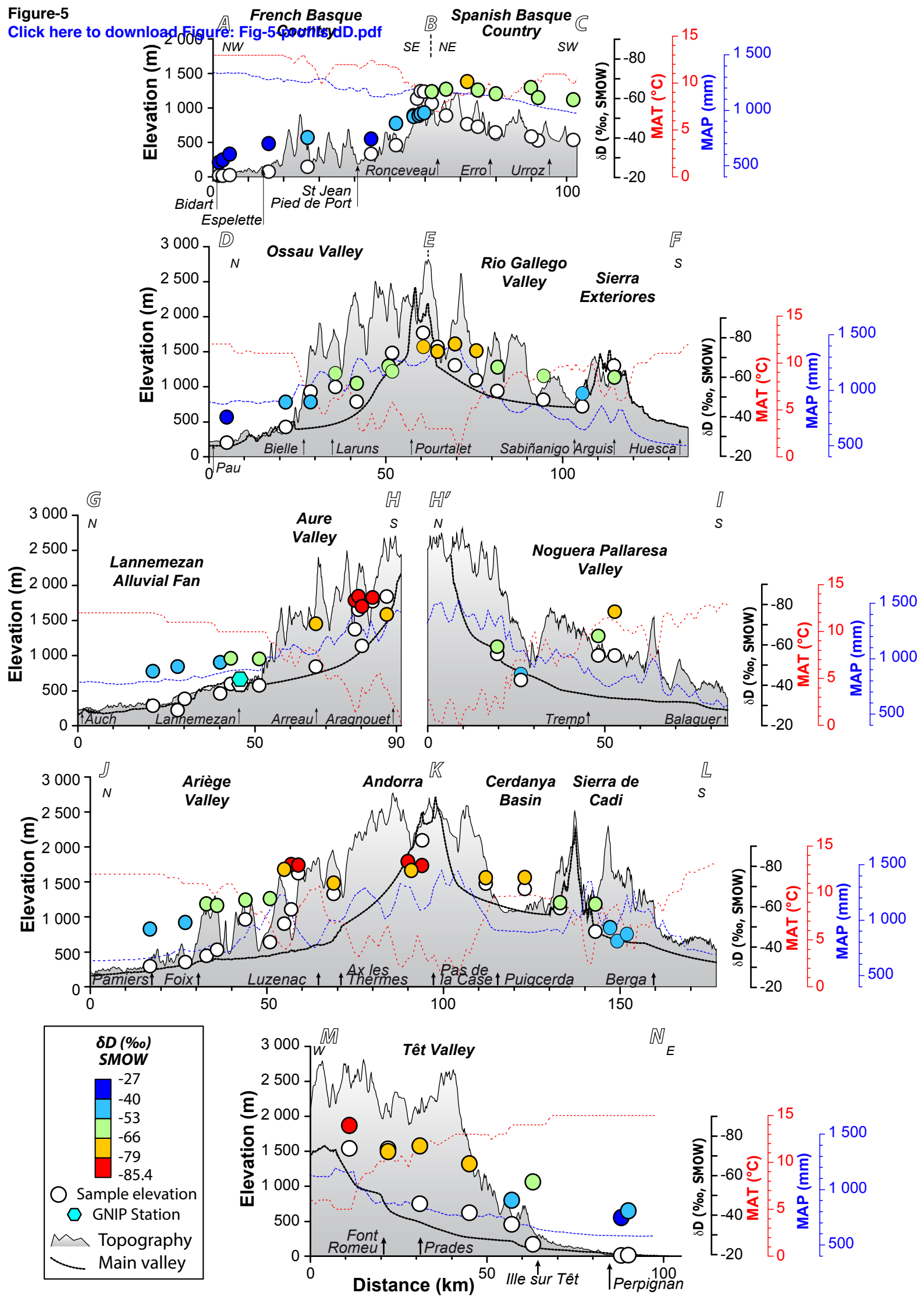

Figure-6

Click here to download Figure: Fig-6-d excess-small.pdf

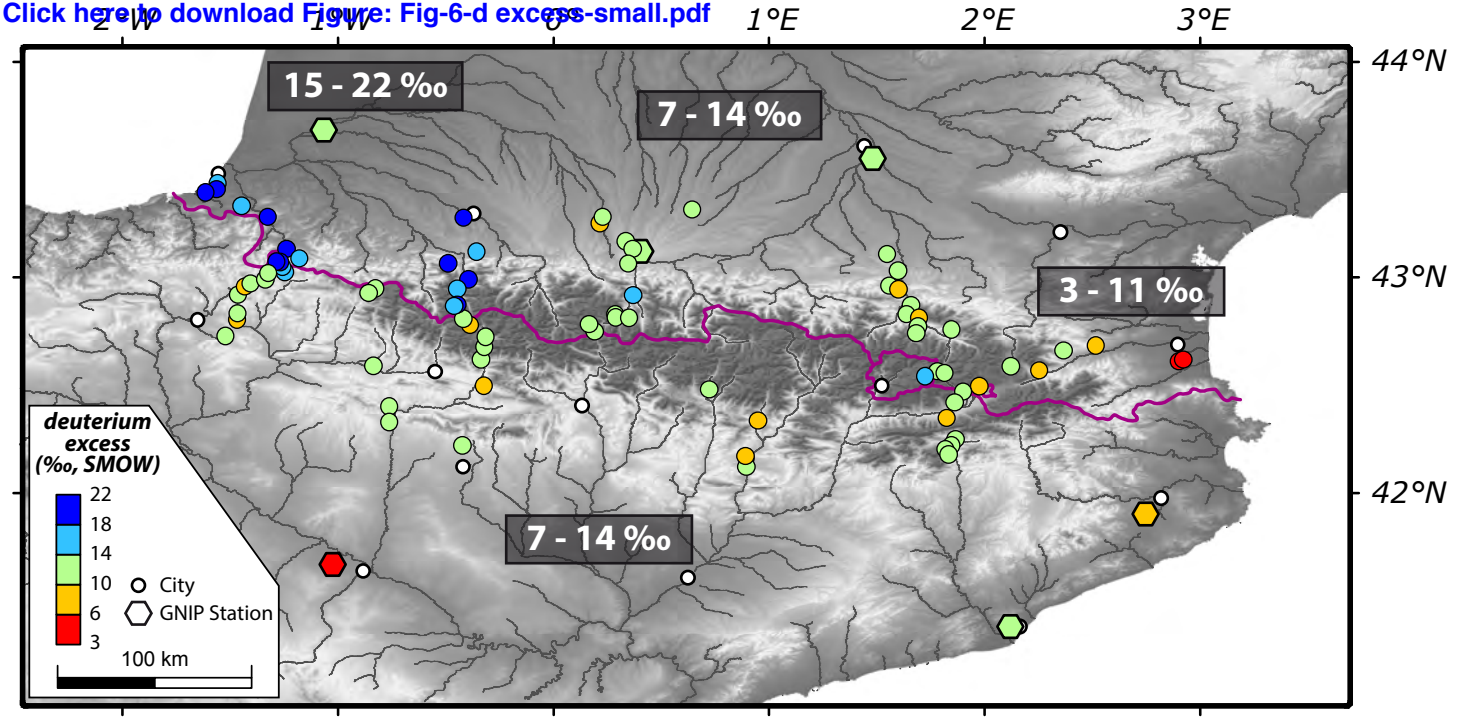

Figure-7

Click here to download Figure: Fig-7-d18O dD rivers-GNIP.pdf

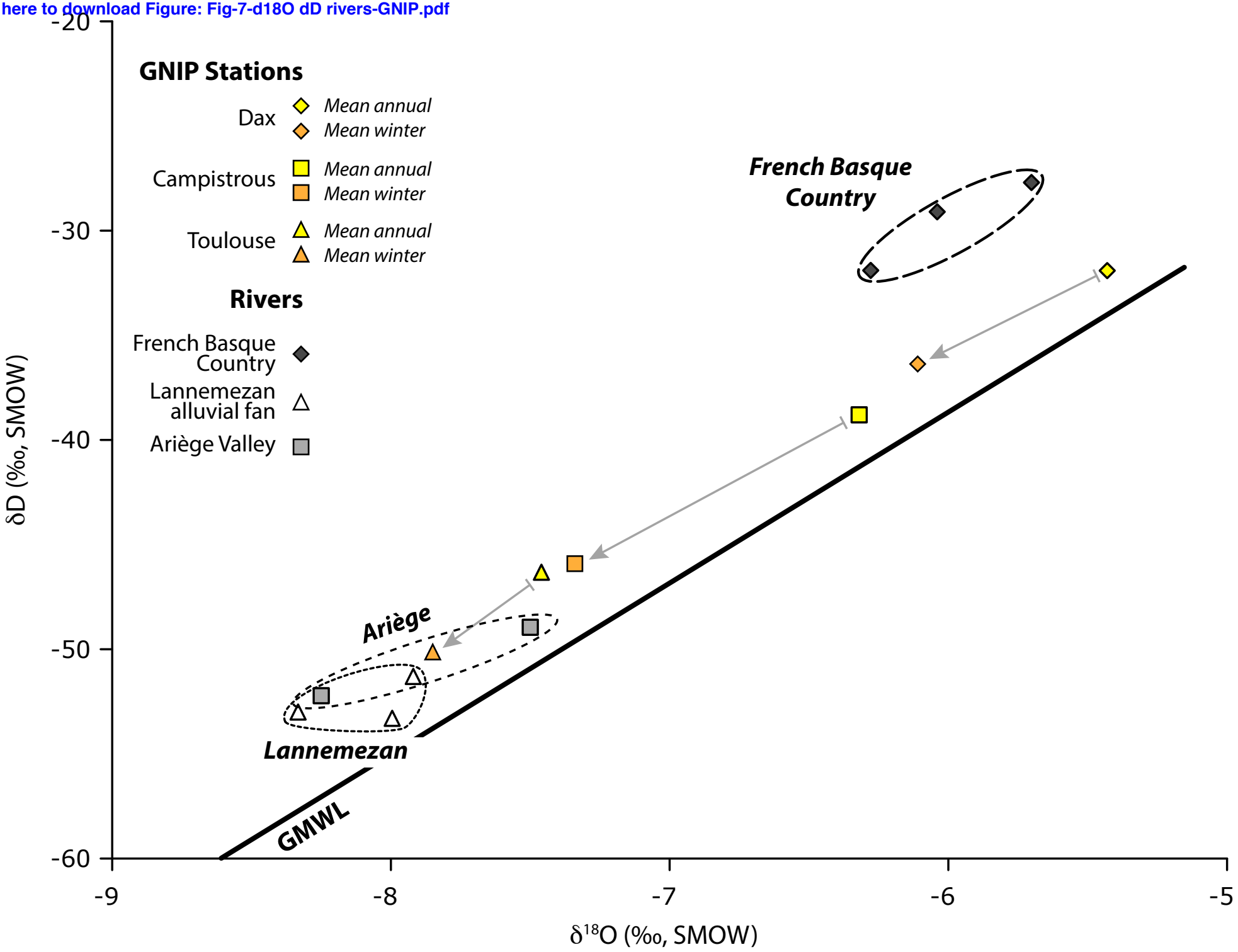

Figure-8

Click here to download Figure: Fig-8 V2.pdf

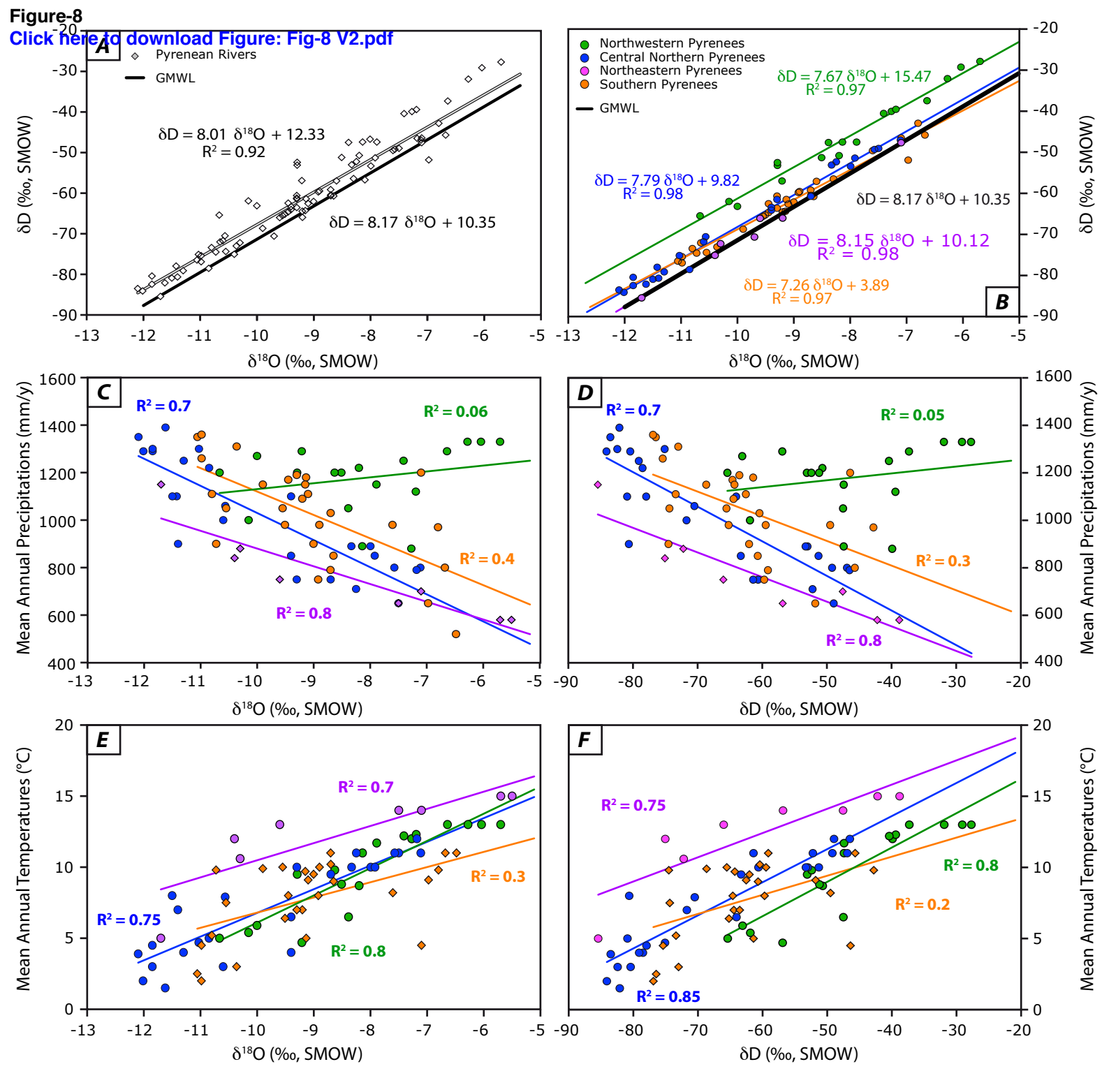

Figure-9

Click here to download Figure: Fig-9-d18O-Alt-Pyr.pdf

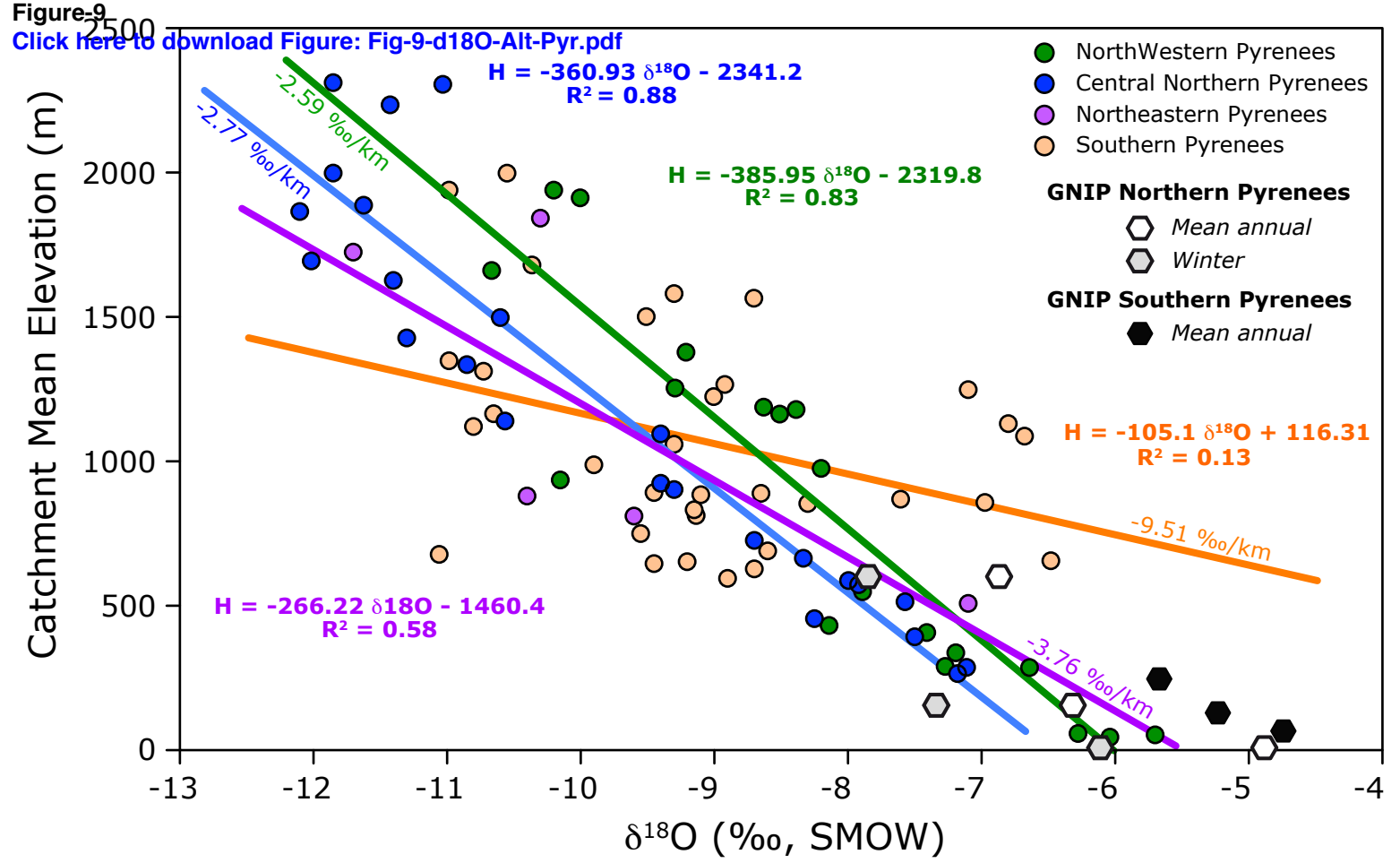

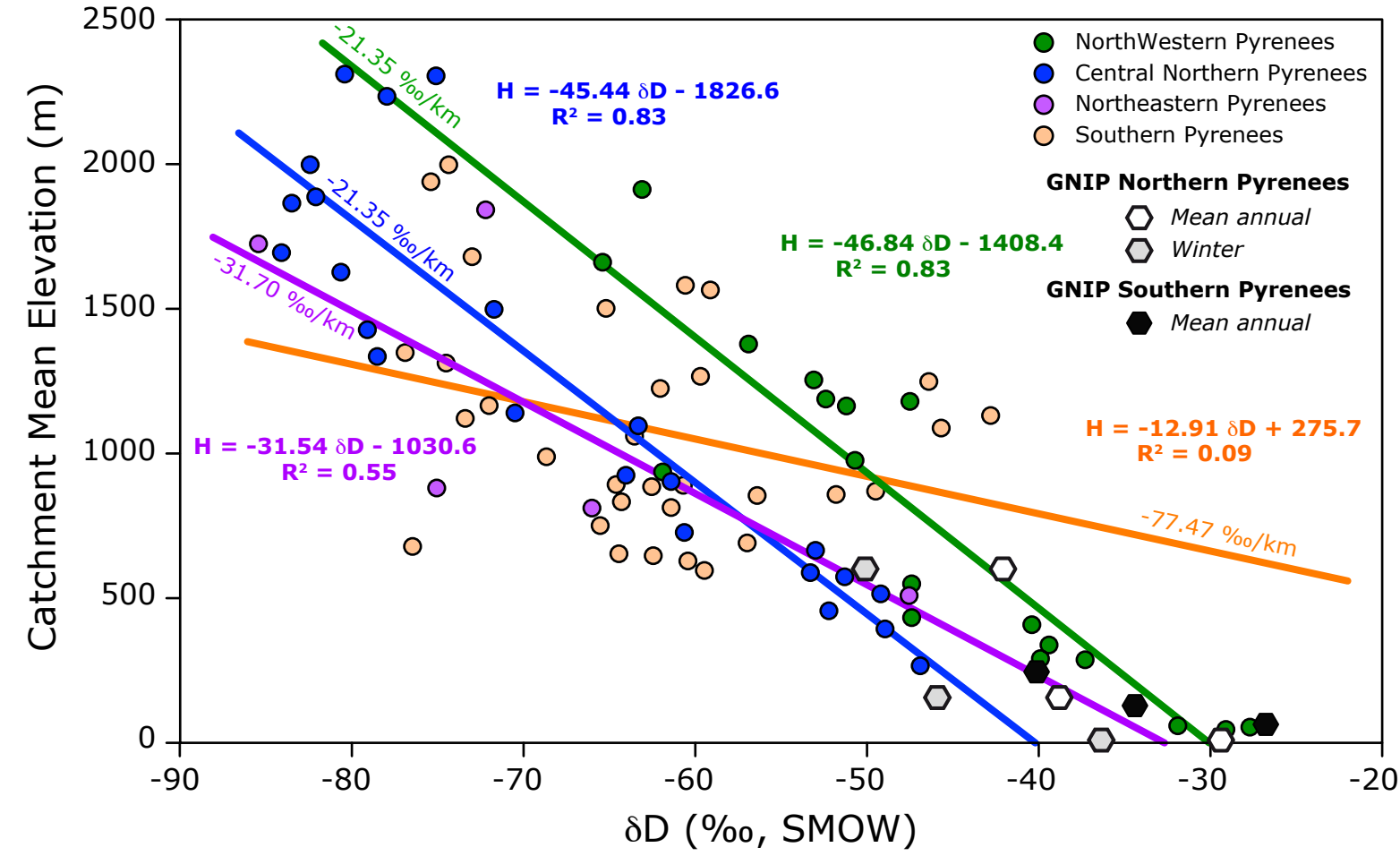

Figure-10

Click here to download Figure: Fig-10-d18O-Alt-Synthse.pdf